Shell model study of single-particle and collective structure in neutron-rich Cr isotopes

K. Kaneko,[1,*] Y. Sun,[2,†] M. Hasegawa,[3] and T. Mizusaki[4]

[1]*Department of Physics, Kyushu Sangyo University, Fukuoka 813-8503, Japan*
[2]*Department of Physics, Shanghai Jiao Tong University, Shanghai 200240, P. R. China*
[3]*Institute of Modern Physics, Chinese Academy of Sciences, Lanzhou 730000, P. R. China*
[4]*Institute of Natural Sciences, Senshu University, Tokyo 101-8425, Japan*

The structure of neutron-rich Cr isotopes is systematically investigated by using the spherical shell model. The calculations reproduce well the known energy levels for the even-even $^{52-62}$Cr and odd-mass $^{53-59}$Cr nuclei, and predict a lowering of excitation energies around neutron number $N = 40$. The calculated $B(E2; 2_1^+ \rightarrow 0_1^+)$ systematics shows a pronounced collectivity around $N = 40$; a similar characteristic behavior has been suggested for Zn and Ge isotopes. Causes for the sudden drop of the $9/2_1^+$ energy in ^{59}Cr and the appearance of very low 0_2^+ states around $N = 40$ are discussed. We also predict a new band with strong collectivity built on the 0_2^+ state in the $N = 40$ isotope ^{64}Cr.

PACS numbers: 21.10.Dr, 21.60.Cs, 21.60.Jz, 21.10.Re

I. INTRODUCTION

The neutron-rich fp-shell nuclei far from the valley of stability are of particular interest in recent experimental and theoretical studies [1]. To provide a satisfactory description of these nuclei, the challenge remains to understand what mechanisms cause changes in nuclear shell structure as neutron number increases in nuclear systems. Theoretical calculations have questioned the persistence of the traditional magic numbers, which have been known to exist in stable nuclei. For example, ^{68}Ni is expected to be a double-magic nucleus as a consequence of the neutron subshell gap separating the fp-shell and $g_{9/2}$ orbital at the neutron number $N = 40$ [2, 3, 4]. The size of this subshell gap is characterized by the excitation across the fp-shell and $g_{9/2}$ orbital [5, 6]. In addition to this, the presence of the positive-parity $g_{9/2}$ orbital above the negative-parity fp shell strongly hinders 1p-1h excitations. This $N = 40$ shell gap, however, disappears when protons are added to or subtracted from ^{68}Ni [7]. It was discussed in Refs. [8, 9] that in the early mean-field calculations, a distinct shell gap that exists in the $N = 40$ nucleus ^{68}Ni disappears when quadrupole correlations are taken into account. Even for ^{68}Ni, it does not show a pronounced irregularity in the two-neutron separation energy as expected for a typical double-magic nucleus. It has been suggested [10] that a small $B(E2, 0_1^+ \rightarrow 2_1^+)$ value is not a strong evidence for the double-magic character. We may thus conclude that the double-magicity nature in ^{68}Ni is still controversial and remains an open question.

On the other hand, collective structure is predicted to develop in neutron-rich nuclei. Zn and Ge nuclei are known to exhibit rather strong collectivity around $N = 40$ [11, 12]. Both unusually low excitation of the first excited 0_2^+ state and strong enhancement of $B(E2; 0_1^+ \rightarrow 2_1^+)$ near $N = 40$ indicate a dramatic structure change at this nucleon number. Recently, we have shown [13] that this characteristic behavior can possibly be understood in terms of rapid increase in the $g_{9/2}$ proton and neutron occupation. However, in order to explain the structure change and enhancement in $B(E2)$, we needed effective quadrupole matrix elements and large effective charges. Shell model calculations [6] have also predicted an excited band in ^{68}Ni based on the 0_2^+ state.

For ^{60,62,64}Cr, shell-model calculations in the fpg-shell space with the ^{48}Ca core (i.e. the ^{40}Ca core and eight $f_{7/2}$ frozen neutrons) have shown [14] that these nuclei are strongly deformed with large quadrupole moments and large $B(E2; 2_1^+ \rightarrow 0_1^+)$ values. The recent report [15] on some even-even Cr isotopes has indicated a lowering of the 2^+ energy beyond $N = 34$. The monopole interaction discussed by Otsuka *et al.* [16, 17] should affect differently the protons occupying the $\pi f_{7/2}$ and $\nu f_{5/2}$ orbitals, and should have an impact on the neutron single-particle spectra involved. However, it has been demonstrated that the $\nu g_{9/2}$ orbital should not be ignored in the description of $N \geq 34$ isotopes. In fact, the GXPF1A interaction [18] in the fp-shell space cannot describe the energy levels in ^{59}Cr and ^{60}Cr [15], and the calculated excitation energies are found much higher than the experimental ones. Sorlin *et al.* [5] suggested an onset of a sizable deformation in ^{60}Cr. Recent observation [15], however, has questioned this interpretation in terms of deformation. Rather, the low-lying energy systematics of neutron-rich Cr isotopes has been discussed in terms of a softening of nuclear shape with increasing neutron number.

The low-lying $9/2_1^+$ states in odd-mass neutron-rich Cr isotopes are obviously outside the fp-shell model space. The recent observation [19] in some odd-mass neutron-rich Cr isotopes reveals that the $9/2_1^+$ state energy drops down considerably with increasing neutron number. The

*Electronic address: kaneko@ip.kyusan-u.ac.jp
†Electronic address: sunyang@sjtu.edu.cn

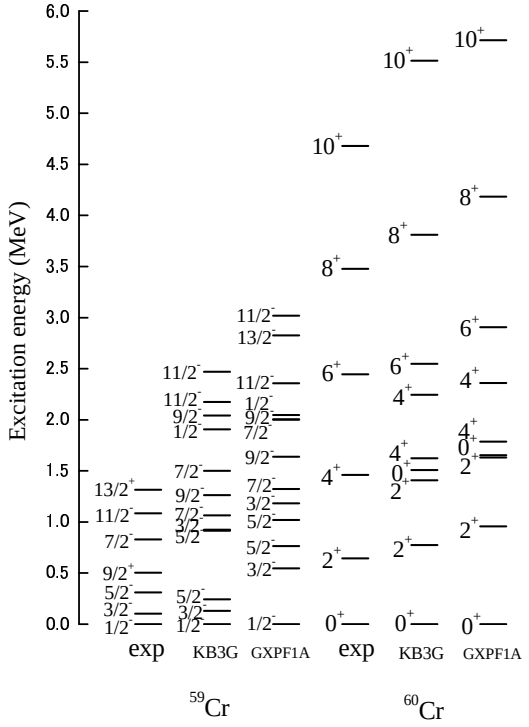

FIG. 1: Comparison of experimental energy levels with the KB3G and the GXPF1A calculations for ^{59,60}Cr.

sharp decrease of the $9/2^+_1$ state energy is considered as a clear indication for the monopole interaction, and the attractive force between the $1g_{9/2}$ and $2p_{3/2}$ neutron orbitals pushes down the $1g_{9/2}$ orbital. The mean-field calculations suggested the presence of prolately-deformed rotational bands built on the $g_{9/2}$ states in ^{55,57}Cr, while the long-lived $g_{9/2}$ isomeric state observed in ^{59}Cr was considered to be consistent with an oblate deformation [20, 21]. All these indicate that different shapes may coexist and a shape change may occur in ^{59}Cr. The abrupt change in structure of odd-mass neutron-rich Cr isotopes can be better explained by the appearance of the $g_{9/2}$ orbital at low energy. The observation of the $9/2^+_1$ state at low-excitation energy undoubtedly demonstrates the necessity of including the $g_{9/2}$ orbital in the calculation.

When these neutron-rich nuclei rotate faster, it is required also to involve the $g_{9/2}$ orbital to discuss the physics. The study of high-spin states in the even-even ^{56,58,60}Cr isotopes is important to gain information about the evolution of single-particle and collective excitations. A comparison of the high-spin data with current shell model calculations indicates that there is strong motivation for extending the interactions to include the neutron $g_{9/2}$ orbital [15]. Thus, a consistent approach to the structure study in this mass region would suggest that the $g_{9/2}$ orbital should drive toward collectivity in the neutron-rich Cr isotopes for $N \geq 34$.

In Fig. 1, we compare the experimental energy levels of ^{59}Cr and ^{60}Cr with the present calculation, and with calculations using the GXPF1A and KB3G interactions. It has recently been discussed [15] that the GXPF1A interaction [18] is inadequate to describe the neutron-rich Cr isotopes beyond $N = 34$. For example, for ^{59}Cr their calculated energy levels of the low-lying negative-parity states lie much higher than what are seen in the data, and the discrepancy is further amplified in higher spin yrast states. While their results for the $N \leq 34$ Cr isotopes reproduce the data, the agreement with the even-even ^{60}Cr data is poor for high-spin states. To understand the single-particle and collective structure in neutron-rich Cr isotopes, shell-model calculations in a full fpg-shell space are highly desirable. However, conventional shell-model calculations in the full fpg-shell space are not possible at present because of too huge dimensions in the configuration space. For neutron-rich Cr isotopes, we have to restrict the model space to the fpg model space of ^{48}Ca, namely, using the ^{40}Ca core with eight $f_{7/2}$ frozen neutrons. In the $N = 40$ region, the $d_{5/2}$ orbital may need to be taken into account to develop quadrupole collectivity [13, 14, 22, 23]. However, recent observations in ^{80}Zn [12] and ^{82}Ge [11] indicate the persistence of the $N = 50$ shell gap, implying that the $d_{5/2}$ orbital may not affect much the collectivity of the neutron-rich Cr isotopes with $N \leq 50$.

In the present work, we perform large-scale spherical shell model calculations using the pairing plus multipole forces with the monopole interaction included [24, 25]. The fpg model space comprises the $0f_{7/2}$, $1p_{3/2}$, $0f_{5/2}$, $1p_{1/2}$ active proton orbitals and $0f_{7/2}$, $1p_{3/2}$, $0f_{5/2}$, $1p_{1/2}$, $0g_{9/2}$ neutron orbitals with eight $f_{7/2}$ frozen neutrons. Structure of neutron-rich Cr isotopes will be investigated in detail. In particular, the interplay between single-particle and collective properties will be discussed.

The paper is arranged as follows. In Section II, we outline our model. In Section III, we present the results from numerical calculations and discuss them for a long chain of Cr isotopes. Finally, conclusions are drawn in Section IV.

II. THE SHELL MODEL

We start with the following form of Hamiltonian, which consists of pairing plus multipole terms with the monopole interaction included:

$$\begin{aligned} H &= H_{\rm sp} + H_{P_0} + H_{P_2} + H_{QQ} + H_{OO} + H^{T=0}_{\pi\nu} + H_{\rm mc} \\ &= \sum_\alpha \varepsilon_a c^\dagger_\alpha c_\alpha - \sum_{J=0,2} \frac{1}{2} g_J \sum_{M\kappa} P^\dagger_{JM1\kappa} P_{JM1\kappa} \\ &- \frac{1}{2}\chi_2/b^4 \sum_M : Q^\dagger_{2M} Q_{2M} : - \frac{1}{2}\chi_3/b^6 \sum_M : O^\dagger_{3M} O_{3M} : \\ &- k^0 \sum_{a\leq b} \sum_{JM} A^\dagger_{JM00}(ab) A_{JM00}(ab) \\ &+ \sum_{a\leq b} \sum_T k^T_{\rm mc}(ab) \sum_{JMK} A^\dagger_{JMTK}(ab) A_{JMTK}(ab), \quad (1) \end{aligned}$$

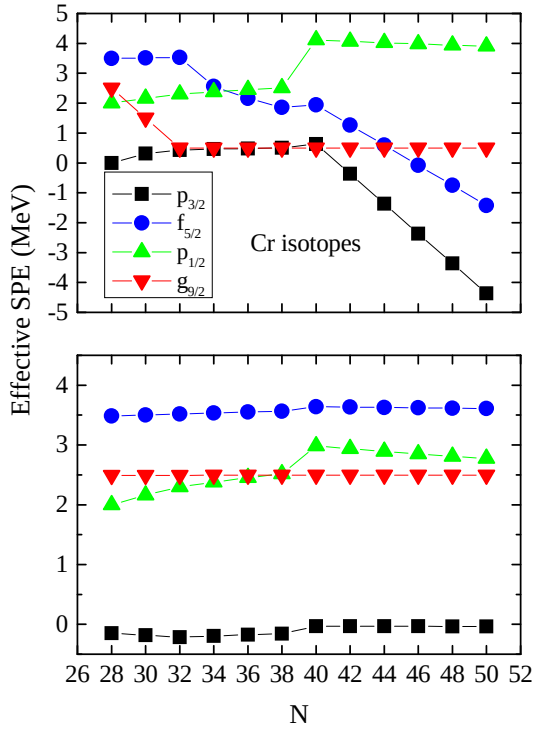

FIG. 2: (color online) Effective single-particle energies e_α for even-even Cr isotopes. (Upper panel) calculation from the shell-model Hamiltonian with the monopole interactions, and (lower panel) without the monopole interactions.

where b in the third and fourth terms is the length parameter of harmonic oscillator. We take the $J = 0$ and $J = 2$ interactions in the pairing channel, and the quadrupole-quadrupole (QQ) and octupole-octupole (OO) terms in the particle-hole channel [24, 25]. The monopole interaction is divided into two parts, namely the average $T = 0$ monopole field $H_{\pi\nu}^{T=0}$ and the monopole correction term $H_{\rm mc}$. The Hamiltonian (1) is isospin invariant.

Our calculation has been performed by using the ANTOINE shell-model code [26]. We consider the ^{48}Ca core as mentioned above, and employ the single-particle energies $\varepsilon_{f7/2} = 0.0$, $\varepsilon_{p3/2} = 2.0$, $\varepsilon_{p1/2} = 4.0$, $\varepsilon_{f5/2} = 5.5$ (all in MeV) in the calculation. The relative single-particle energies of $f_{7/2}$, $p_{3/2}$, $p_{1/2}$, and $f_{5/2}$ are taken from the excitation energies of the low-lying negative-parity states in ^{49}Ca, and the energy between $\varepsilon_{f7/2}$ and $\varepsilon_{p3/2}$ is determined from the excitation energy of $3/2^-$ state in ^{41}Ca. The single-particle energy $\varepsilon_{g9/2} = 4.5$ MeV is chosen so as to reproduce the $9/2^+_1$ energy level in ^{53}Cr. It is not surprising that the $g_{9/2}$ orbit lies below the $f_{5/2}$ orbit because the $9/2^+$ level is lower than the $5/2^-$ level in ^{49}Ca [31]. This lowering of the $g_{9/2}$ would be attributed to the attractive $T = 1$ monopole interaction $V^{T=1}_{f_{7/2},g_{9/2}}$.

We adopt the following interaction strengths for the pairing plus multipole forces

$$g_0 = 17.89/A, \quad g_2 = 152.24/A^{5/3},$$
$$\chi_2 = 228.36/A^{5/3}, \chi_3 = 485.1/A^2 \text{ (in MeV)}. \quad (2)$$

The average monopole force $H_{\pi\nu}^{T=0}$ is neglected because it does not affect the low-lying excited states of neutron-rich Cr isotopes. For the monopole correction terms, we use

$$k_{\rm mc}^{T=0}(f_{7/2}, p_{3/2}) = 0.5, \quad k_{\rm mc}^{T=0}(f_{7/2}, f_{5/2}) = -0.6,$$
$$k_{\rm mc}^{T=0}(f_{7/2}, p_{1/2}) = 0.4, \quad k_{\rm mc}^{T=1}(p_{3/2}, g_{9/2}) = -1.0(3)$$

The repulsive $\pi f_{7/2}$-$\nu p_{3/2}$ and $\pi f_{7/2}$-$\nu p_{1/2}$ monopole interactions can give rise to the correct order of energy levels in odd-mass Cr isotopes, and also lower the first excited 0^+_2 state for the even-even Cr nuclei near $N = 28$. From comparison of the low-lying levels of ^{49}Ca with those of ^{57}Ni, one sees clearly that the $5/2^-_1$ state in ^{57}Ni requires a monopole interaction between $\pi f_{7/2}$ and $\nu f_{5/2}$. This interaction also plays an important role in lowering the first excited 0^+_2 state around $N = 40$. The sharp decrease [20] of the low-lying $9/2^+_1$ state observed along the isotopic chain from ^{53}Cr to ^{59}Cr is considered as a clear indication for the monopole interaction, and the attraction between the $\nu p_{3/2}$ and $\nu g_{9/2}$ orbitals pushes down the $9/2^+_1$ state. Having considered the above monopole interactions, we choose the single-particle energy of the $g_{9/2}$ orbital so as to reproduce the $9/2^+_1$ energy in ^{53}Cr. For calculations of spectroscopic Q-moments and $B(E2)$ values, we take the standard effective charges $e_\pi = 1.5e$ for protons and $e_\nu = 0.5e$ for neutrons.

To get insight of the characteristic behavior of these neutron-rich Cr isotopes, we further consider mean-field approximations for our shell model Hamiltonian. The so-obtained effective single-particles are the dressed particles that carry information on the interactions. In Fig. 2, we present the calculated neutron effective single-particle energies (SPE) [6]. The upper (lower) panel in Fig. 2 shows the effective SPE in the shell-model Hamiltonian (1) with (without) the monopole interactions (3). In the upper panel, we can see drastic variations of the effective SPE for each orbitals.

First, starting from $N = 28$, the effective SPE for the $g_{9/2}$ orbital decreases quickly with increasing neutron number, and then becomes degenerate with the $p_{3/2}$ orbital in the range from $N = 32$ to $N = 40$. The sudden drop of the first excited $9/2^+_1$ in the odd-mass nuclei $^{53-59}$Cr (see later in Figs. 5 and 6) is related to this behavior of $g_{9/2}$, while the pairing correlation increases the excitation energy of $9/2^+_1$ by about 1 MeV. This rapid decrease of the effective SPE is attributed to the strong attractive monopole interaction between the $\nu p_{3/2}$ and $\nu g_{9/2}$ orbitals in Eq. (3).

Second, we can see a change of the SPE level spacings among the orbitals around $N = 40$. This change is also due to the monopole interactions in Eq. (3). The repulsive $\pi f_{7/2}$-$\nu p_{3/2}$ and $\pi f_{7/2}$-$\nu p_{1/2}$ monopole interactions

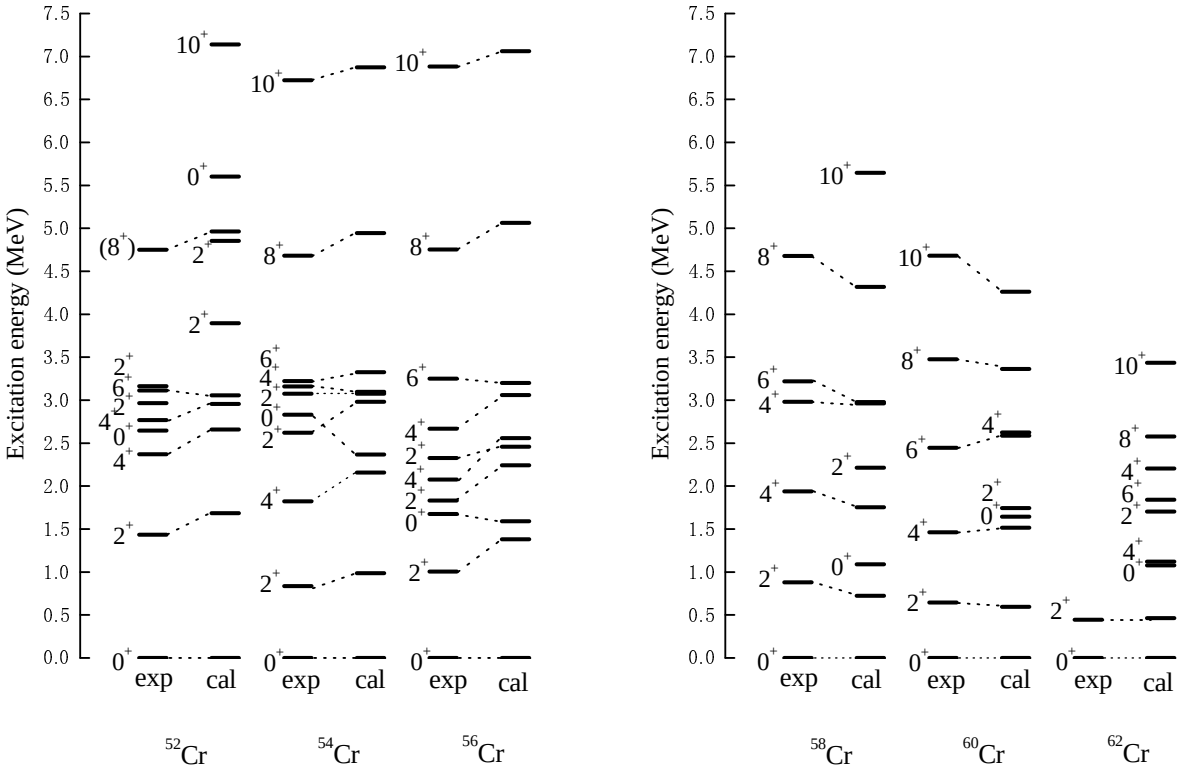

FIG. 3: Experimental and calculated energy levels of positive-parity states for even-even isotopes $^{52-62}$Cr.

give a correct sequence of the energy levels in odd-mass Cr isotopes. The attractive $\pi f_{7/2}$-$\nu f_{5/2}$ monopole interaction plays an important role in lowering the first excited 0_2^+ state around $N = 40$. As already mentioned before, the attraction between the $\nu p_{3/2}$ and $\nu g_{9/2}$ orbitals pushes down the $9/2_1^+$ state, and provides an explanation for the sharp decrease of the low-lying $9/2_1^+$ state from ^{53}Cr to ^{59}Cr. These monopole interactions cooperatively give rise to the reduction of the effective SPE spacing. The deformation that develops around $N = 40$ is due to the quasi-degeneracy of the effective SPE spacing and the collectivity of the intruder $\nu g_{9/2}$ orbital.

III. RESULTS AND DISCUSSIONS

A. Energy levels

Let us first present the shell model results for even-even Cr isotopes. Figure 3 shows a comparison between calculated results for positive-parity states and the experimental data [15, 31] for the even-even Cr isotopes $^{52-62}$Cr. As one can see, the theoretical results describe satisfactorily the experimental energy levels. The feature that the first excited 2_1^+ energy is steadily decreasing as neutron number approaching $N = 40$ is correctly reproduced. One can also see a local increase of 2_1^+ energy at ^{56}Cr.

The calculated first excited 0_2^+ states for $^{52-56}$Cr show a decreasing trend with increasing neutron number, although the calculated 0_2^+ energy for ^{52}Cr lies too high as compared to experiment. This discrepancy may be caused by the assumption of the $N = 28$ shell closure in the present calculation. The neutron excitations of the $N = 28$ core, which are neglected in the present study, would lower the 0_2^+ state in ^{52}Cr. The situation is quite similar to the anomalous behavior of the 0_2^+ state in ^{54}Fe. In fact, the full fp-shell model calculation [32] has shown that the 0_2^+ states in ^{52}Cr and ^{54}Fe are the 2p-2h bandhead. The present calculation predicts the 0_2^+ energy levels in $^{58-62}$Cr which have not yet been observed. It is interesting to see a particular prediction that the calculated 0_2^+ level jumps up at ^{60}Cr with $N = 36$ while the 2_1^+ level in the same nucleus decreases. The attractive $\nu p_{3/2}$-$\nu g_{9/2}$ monopole interaction pushes the $g_{9/2}$ orbital down, causing the single-particle spacing between the $g_{9/2}$ and the $p_{1/2}$ orbital to increase.

Figure 4 shows a comparison between the calculated

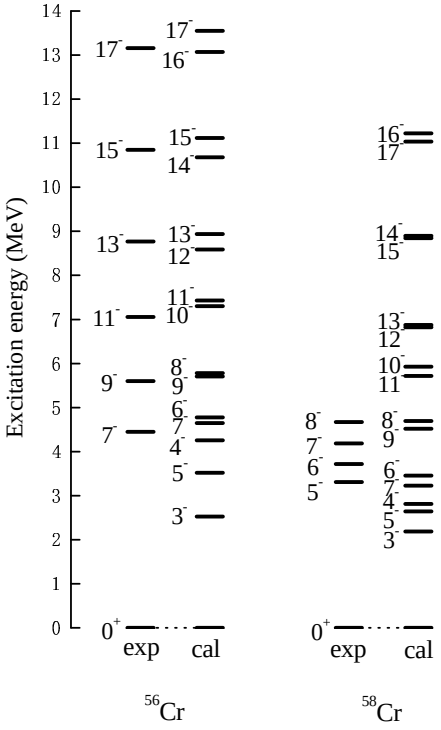

FIG. 4: Experimental and calculated energy levels of negative-parity states for ^{56,58}Cr.

and experimental energy levels for the negative-parity states in ^{56}Cr and ^{58}Cr [15]. In ^{56}Cr, the odd-spin levels of 7^-_1, 9^-_1, 11^-_1, 13^-_1, 15^-_1, and 17^-_1 are reproduced very well, while the even-spin levels are predicted. The 3^-_1 states in ^{56}Cr and ^{58}Cr are predicted to lie around 2.5 MeV. The 3^-_1 state is considered as an 1p-1h excitation from the negative-parity orbital $p_{3/2}$ to the positive parity orbital $g_{9/2}$ because the 3^-_1 energies are comparable to the single-particle spacing 2.5 MeV between these orbitals. In addition, it is interesting to see a predicted formation of spin doublet states in both nuclei, as for instance the pairs 10^-_1-11^-_1, 12^-_1-13^-_1, 14^-_1-15^-_1, and 16^-_1-17^-_1. In ^{58}Cr, the even-spin levels of 6^- and 8^- are reproduced well, although the calculated odd-spin 5^-_1 and 7^-_1 levels are lower than the experimental ones.

In Fig. 5, calculated results for the odd-mass Cr isotopes $^{53-59}$Cr are shown, and compared with experimental data [15, 31]. Overall, the calculation reproduces the data well. In particular, the agreement for ^{53,55}Cr with both negative- and positive-parity states is excellent. In ^{57}Cr, most energy levels are described well; only the low-lying $5/2^+_2$ and $7/2^+_1$ states are calculated higher than the experimental ones. In these odd-mass Cr isotopes, the most striking feature is that the first excited $9/2^+_1$ state drops down rapidly when neutrons are added: from 2087 kev in ^{55}Cr to 1057 kev in ^{57}Cr, and down to 503 kev in ^{59}Cr. The calculation reproduces this systematics very well. This rapid decrease of the $9/2^+_1$ excitation energy can be understood as due to the attractive monopole interaction between the $\nu g_{9/2}$ and $\nu p_{3/2}$ orbitals that pushes down the $\nu g_{9/2}$ orbital. The high-spin states with positive-parity in ^{55,57}Cr are also reproduced well. In both nuclei, the rotational bands built on the $9/2^+_1$ state provide a strong experimental evidence for the shape-driving potential of this intruder level [19, 20]. In fact, we can see large $E2$ transitions in this band in later discussions.

At this point, it is worthwhile discussing systematics of the $9/2^+_1$ state. In Fig. 6, the $9/2^+_1$ states of the odd-mass Cr are compared with those of Fe, Ni, Zn, and Ge isotopes [31]. As already seen from Fig. 5, the calculated energy levels of $9/2^+_1$ are in a good agreement with experiment for $^{53-59}$Cr. Now in Fig. 6, all the curves show that the $9/2^+_1$ state energy steadily decreases with increasing neutron number. It should be pointed out that the more rapid drop of the $9/2^+_1$ energy from ^{57}Cr to ^{59}Cr correlates with the sudden increase of the calculated 0^+_2 energy from ^{58}Cr to ^{60}Cr in Fig. 3. Further calculations beyond $N = 37$ predict a low-excited $9/2^+_1$ for $^{61-65}$Cr. Interestingly enough, the curve for Cr isotopes is found to be very close to that of Ge isotopes, namely, the odd-mass Cr and Ge isotones have very similar $9/2^+_1$ energy. At $N = 41$, the $9/2^+$ state becomes the ground state for ^{69}Ni and^{73}Ge, while it is an excited state at 0.158 MeV for ^{71}Zn. The calculation predicts that the $9/2^+_1$ level is an excited state for ^{65}Cr.

In Fig. 7, we compare the experimental energy levels of ^{59}Cr and^{60}Cr with the present and the GXPF1A calculation. Our results in Fig. 7, as well as in the early discussed Fig. 3, show a much better agreement. The present calculation reproduces the positive-parity $9/2^+_1$ and $13/2^+_1$ states in ^{59}Cr, and predicts higher-spin states above them. For ^{60}Cr, our calculation nicely reproduces the experimental high-spin levels as well. It is thus clear that the $\nu g_{9/2}$ excitations play a significant role in the current problem, and it is crucial to include this orbital for a correct description of these nuclei.

The above success motivates us to move in on the even more neutron-rich region, where no experimental data are available. Let us next investigate the Cr isotopes beyond $N = 38$. Recent observation of very low first excited 2^+ states in ^{60}Cr and ^{62}Cr suggests that these nuclei are deformed [5]. We thus expect that collective motion may be the dominant mode for the low-lying states in the isotopes around $N = 40$. Figure 8 shows the calculated energy levels of yrast states for the neutron-rich even-even isotopes $^{52-74}$Cr. For those below $N = 36$, the calculated results reproduce well the observed trend of experimental data. In ^{56}Cr, the calculation correctly reproduces the enhanced excitation energy of the first excited 2^+_1 and 4^+_1 state as compared with the corresponding states in the neighboring ^{54,58}Cr, which is, as discussed early, a strong signature of the subshell gap at $N = 32$.

There is a striking behavior along the isotopic chain: the abrupt change in structure at $N = 36$ in ^{60}Cr. As can be clearly seen from Fig. 8, the 6^+_1, 8^+_1, and 10^+_1 state energies drop down suddenly at this neutron number. Another notable structure change, as shown in Fig. 9, is

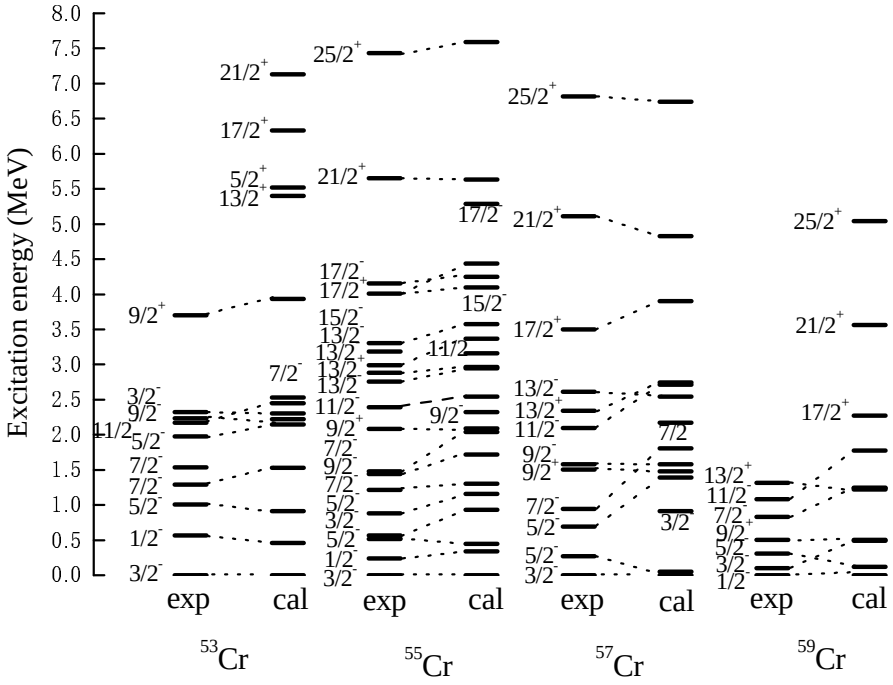

FIG. 5: Experimental and calculated energy levels for the odd-mass $^{53-59}$Cr.

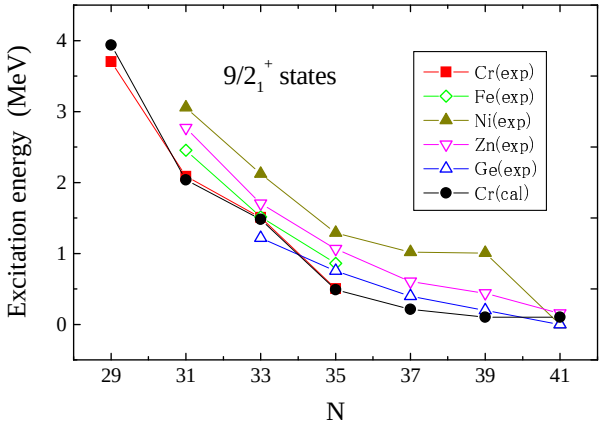

FIG. 6: (Color online) Systematics of the first excited $9/2_1^+$ states for Cr, Fe, Ni, Zn, and Ge isotopes. The calculated energy levels are compared with experimental data for odd-mass Cr nuclei.

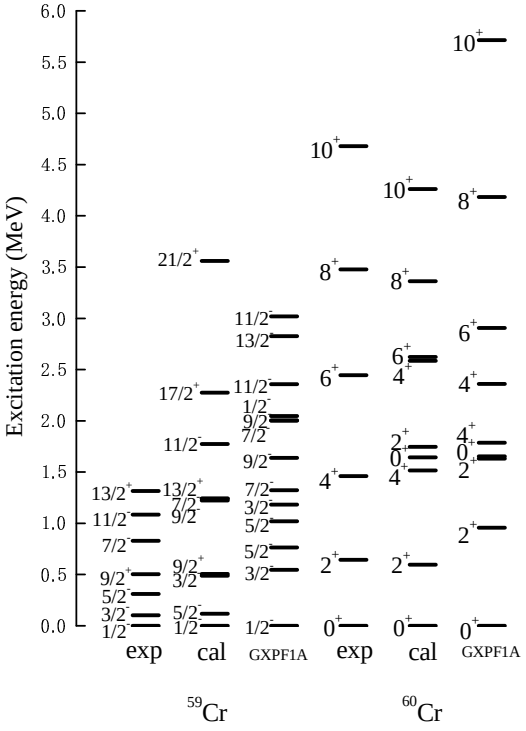

FIG. 7: Comparison of experimental energy levels with the present and the GXPF1A calculations for ^{59,60}Cr.

that the excitation energy of the 0_2^+ state exhibits a peak at $N = 36$. Remarkably, a similar structure evolution has been seen along the $N = Z$ line in the proton-rich region, and a abrupt change in structure in the $N = Z = 36$ nucleus ^{72}Kr has been discussed [33] by the present authors. In Ref. [33], it was discussed that the yrast energy levels in the $N = Z < 36$ nuclei ^{64}Ge and ^{68}Se show larger separations, corresponding to smaller moments of inertia, but in ^{72}Kr, the level separation in the yrast sequence goes down drastically. We have suggested in Ref. [33] that this is an example of phase transition along the $N = Z$ line.

We now discuss the isotopes beyond $N = 36$. In the $N = 38$ isotope ^{62}Cr, only the first excited 2_1^+ state has been observed [14]. Together with this state, a general trend starting from $N = 32$ can be clearly seen, in which

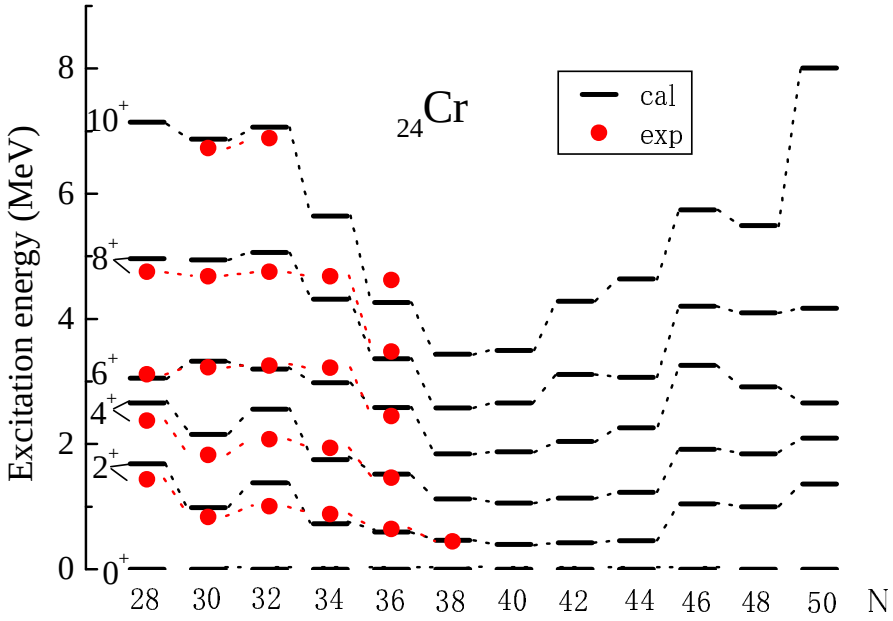

FIG. 8: (color online) Experimental and calculated energy levels of the yrast states for the even-even Cr isotopes with $N = 28 - 50$.

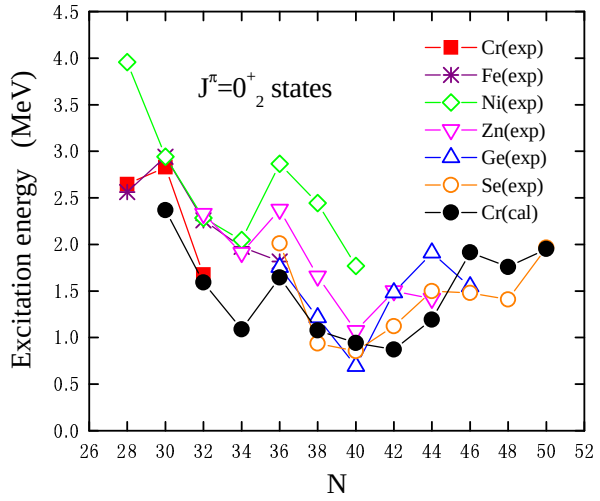

FIG. 9: (color online) Systematics of the first excited 0^+_2 states for Cr, Fe, Ni, Zn, Ge, and Se isotopes. The calculated energy levels are compared with the experimental data for Cr isotopes.

the 2^+_1 excitation energies decrease gradually with increasing neutron number. The calculated excitation energies of yrast states further drop down at the $N = 38$ and 40 isotopes. The abrupt changes in structure across neutron-rich Cr isotopes appear as a result of low single-particle level density, which leads to a well-developed deformation at $N = 40$. When going toward more neutron-rich region from $N = 40$ excitation energies of the yrast states begin to increase with increasing neutron number, which makes the $N = 40$ isotope ^{64}Cr the most deformed among the isotopic chain. It was proposed by Zuker *et al.* [22] that a minimal valence space to be able to develop quadrupole collectivity should contain at least a $(j, j-2, ...)$ sequence of orbits. In the upper $g_{9/2}$-shell nuclei, the $g_{9/2}$ orbital and its quasi-SU(3) counterpart the $d_{5/2}$ orbital have to be taken into account in order to reproduce experimental data. Therefore, to describe the neutron upper $g_{9/2}$-shell nuclei, it would be better to take into account the $d_{5/2}$ orbital. At present, however, it is not possible to include the $d_{5/2}$ orbital to the shell model space because of huge dimensions of the configuration space.

In Fig. 9, we show the calculated and experimental 0^+_2 states for even-even Cr isotopes, and for comparison, the experimentally known 0^+_2 states for even-even Fe, Ni, Zn, Ge, and Se isotopes [31] are also plotted. For the only three Cr isotopes for which data exist, the calculation reproduces the data of ^{54,56}Cr. The calculated 0^+_2 level at 5.6 MeV for ^{52}Cr (not shown in Fig. 9) lies too high when compared with the experimental one. The reason for this discrepancy may be attributed to the fact that neutrons in the $f_{7/2}$ orbital are frozen in the calculation. From the systematics in Fig. 9, we can see two characteristics for these first excited 0^+_2 levels. One is the presence of a peak at $N = 36$ in the experimental data for Ni and Zn isotopes as well as in the calculated results for Cr isotopes. For Ge and Se isotopes, $N = 36$ might also show a 0^+_2 peak; however, it is not conclusive at present because there are no data for the 0^+_2 energy at $N = 34$. The other characteristic in Fig. 9 is the occurrence of a minimum in the 0^+_2 energy level around $N = 40$. This minimum occurs because of the monopole interaction between $\pi f_{7/2}$ and $\nu f_{5/2}$.

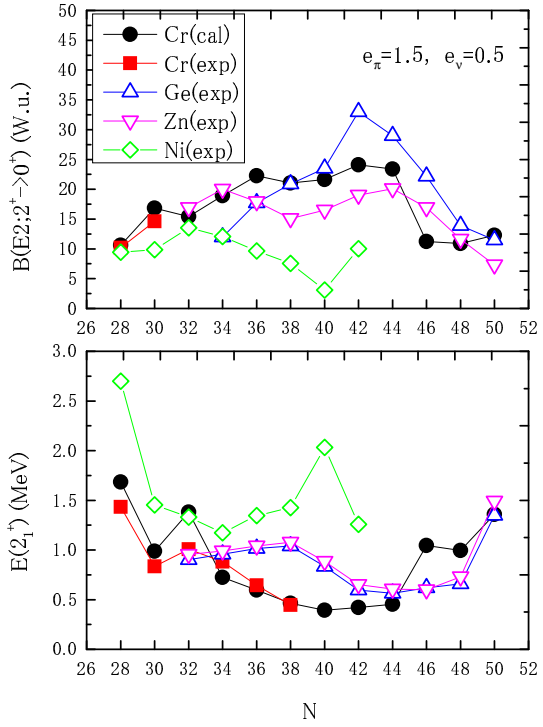

FIG. 10: (color online) Calculated and experimental values of (upper panel) $B(E2, 0_1^+ \rightarrow 2_1^+)$, and (lower panel) $E(2_1^+)$ for even-even Cr, Ni, Zn, and Ge isotopes.

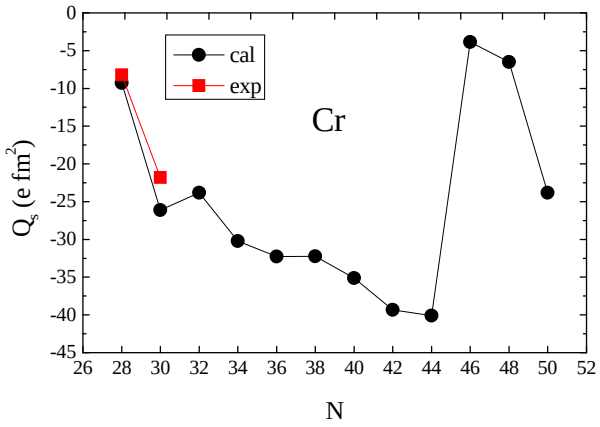

FIG. 11: (color online) Calculated and experimental spectroscopic qudrupole moment for even-even Cr isotopes.

B. $B(E2)$ values

Calculation of electromagnetic transition probabilities serves as a strict test for wave functions of theoretical models. In the upper panel of Fig. 10, experimental $B(E2; 2_1^+ \rightarrow 0_1^+)$ dada for even-even Cr, Ni, Zn, and Ge isotopes are collected [11, 12, 31], and our shell-model calculations for Cr isotopes are compared with the known data. In lower panel of Fig. 10, excitation energies of the first 2^+ state $E(2_1^+)$ are plotted. With the usual effective charges $e_\pi = 1.5e$ and $e_\nu = 0.5e$, the present calculation including the $\pi f_{7/2}$ orbital in the model space is found in good agreement with data for ^{52,54}Cr. A sharp contrasting behavior between Ni and other isotopes can be clearly seen around $N = 40$. The unusual $B(E2)$ and $E(2_1^+)$ behavior near ^{68}Ni shows up at the subshell closure $N = 40$. The $B(E2)$ values around $N = 40$ are determined by filling the unique parity $\nu g_{9/2}$ orbital and the proton core polarization. The present calculation for Cr isotopes suggests that the predicted trend in $B(E2)$ around $N = 40$ is quite similar to the experimentally known systematics in Zn and Ge isotopes [11, 12].

For shell model calculations in the model space consisting of the $1p_{3/2}$, $0f_{5/2}$, $1p_{1/2}$, $0g_{9/2}$ orbitals for protons and neutrons with an inert ^{56}Ni core, large effective charges $e_\pi = 1.9e$ and $e_\nu = 0.9e$ were used to obtain the experimental $B(E2)$ values for Zn and Ge isotopes [11, 12, 13]. This implies that excitation from the $\pi f_{7/2}$ orbital would be important for obtaining large $B(E2)$ values around $N = 40$ [5]. It should be noted that the calculated $E2$ transitions for ^{60,62,64}Cr yield nearly the same values as the recent shell model calculations in the $fpgd$ space including the $d_{5/2}$ orbital [14], where their $B(E2)$ values are, respectively, 20.64, 20.7, 20.9 W.u. for ^{60,62,64}Cr. The calculated 2_1^+ energies in Ref. [14] diverge from the experimental trend as they remain constant up to $N = 38$ and increase at ^{64}Cr.

The deformation estimated from the calculated $B(E2; 2_1^+ \rightarrow 0_1^+)$ around $N = 40$ is $\beta_2 \sim 0.3$, consistent with those obtained from the empirical formula [14] and the Skyrme HFB calculations [34, 35]. In the lower panel of Fig. 10, we can see the $N = 32$ gap in the Cr isotopes. With increasing neutron number beyond $N = 32$, the first excited 2_1^+ states decrease steadily toward $N = 40$. The 2_1^+ energy systematics of Cr behaves quite differently from Zn and Ge isotopes. The sudden drop in $B(E2)$ values and large 2_1^+ excitation energies for $^{70-74}$Cr may be due to the neglect of the $d_{5/2}$ orbital [5] in the present model space.

Figure 11 shows a comparison for the calculated and experimental spectroscopic quadrupole moments Q_s. The calculated Q_s values for ^{52,54}Cr agree well with the data. The drastic variation in the calculated Q_s values for $^{70-74}$Cr may also be an artefact due to the neglect of the $d_{5/2}$ orbital, which causes variations in the $B(E2)$ values and 2_1^+ energy systematics in these nuclei, as seen in Fig. 10.

In a previous paper [6], we predicted a new band built on the first excited 0_2^+ state in two neutron-rich nuclei ^{68}Ni and ^{90}Zn. The structure of states in this band is dominated by 2p-2h excitations from the fp shell to the intruder $g_{9/2}$ orbital. We expect that an analogous band exists also in ^{64}Cr with $N = 40$. The structure of this anticipated band is quite different from that of the ground state. This happens because the opposite signs of parity between the $g_{9/2}$ orbital and the fp shell do not favor 1p-1h excitations. Figure 12 shows the theoretical level schemes. The predicted $B(E2)$ values for ^{62}Cr and ^{64}Cr are summarized in Table I. One can see strong en-

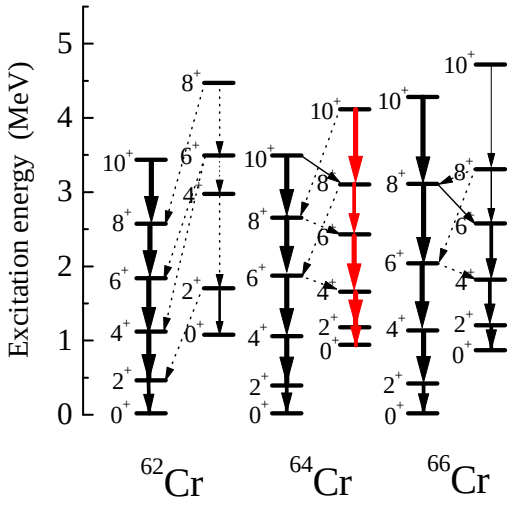

FIG. 12: (color online) Calculated level scheme for ^{62,64,66}Cr. The widths of the arrows denote relative values of $B(E2)$.

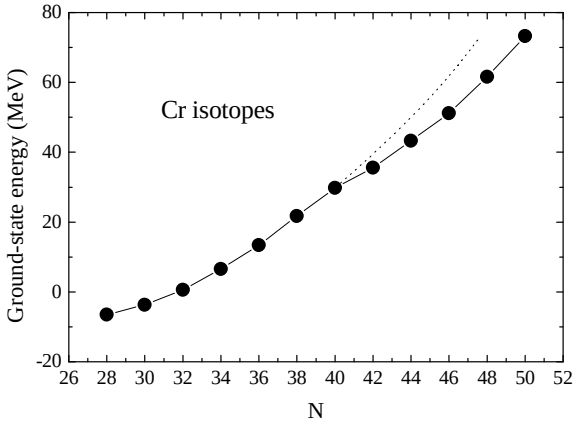

FIG. 13: Ground-state energies in the shell-model calculation for even-even Cr isotopes. The dotted curve is an extrapolation of the lower mass part of the results to show clearly the discontinuity in the slope of the curve at $N = 40$.

hancement in $B(E2)$ values in the side band built on the first excited 0_2^+ state in ^{64}Cr. The $B(E2; 2_1^+ \to 0_1^+)$ and $B(E2; 4_1^+ \to 2_1^+)$ values for ^{62,64}Cr are consistent with the calculated values by Sorlin *et al.* [5]. This situation is very similar to that in the neutron-rich ^{68}Ni and ^{90}Zn. The relevant ingredient here is excitations from the fp shell to the intruder $g_{9/2}$ orbital, and we expect that this is a common feature for the isotones of $N = 40$. In Table II, $B(E2)$ values for the positive-parity band built on the $9/2_1^+$ state in the odd-mass nuclei, $^{53-59}$Cr, are shown. We can see that for ^{59}Cr $E2$ transition rates have large values, and therefore show a strong collectivity. The deformation estimated from the calculated results is $\beta_2 = 0.18$, consistent with the Total Routhian Surface (TRS) calculations [20].

TABLE I: Calculated $B(E2)$ values for the positive-parity yrast states and the excited states in ^{62}Cr and ^{64}Cr. These values are compared with those of Sorlin *et al.* [5].

	^{62}Cr [e^2fm^4]		^{64}Cr [e^2fm^4]	
$I_i^\pi \to I_f^\pi$	Sorlin *et al.*	Calc.	Sorlin *et al.*	Calc.
$2_1^+ \to 0_1^+$	302	307	318	329
$4_1^+ \to 2_1^+$	428	436	471	460
$6_1^+ \to 4_1^+$		449		464
$8_1^+ \to 6_1^+$		455		421
$10_1^+ \to 8_1^+$		500		523
$2_2^+ \to 0_2^+$		243		293
$4_2^+ \to 2_2^+$		5		407
$6_2^+ \to 4_2^+$		17		381
$8_2^+ \to 6_2^+$		7		322
$10_2^+ \to 8_2^+$		335		371

C. Ground-state energies and occupation numbers

It is striking that the effective SPE levels of the $\nu p_{3/2}$ and $\nu f_{5/2}$ orbitals decrease drastically with increasing neutron number beyond $N = 42$. This affects the properties of the ground-state energy in the shell-model calculations. Indeed, as can be clearly seen in Fig. 13, the ground-state energies bend at $N = 40$ so that it exhibits a discontinuity in the slope of the curve in Fig. 13. This would correspond to a kind of phase transition at $N = 40$.

We can look at the above findings with other physical quantities such as neutron occupation numbers of the fpg-shell orbits for the low-lying 0_1^+, 2_1^+, and 0_2^+ levels. The upper panel in Fig. 14 shows occupation numbers for the ground states 0_1^+. For nuclei with smaller N, the main component is of the $\nu p_{3/2}$ orbital. At $N = 36$ and 38, the occupation number for the $\nu g_{9/2}$ orbital increases and nearly equals to that of the $p_{3/2}$ orbital. At $N = 40$, the three occupation numbers of $\nu p_{3/2}$, $\nu g_{9/2}$, and $\nu f_{5/2}$ take almost same values. Going to higher neutron numbers from $N = 40$, occupation number of the $\nu g_{9/2}$ orbital increases drastically and becomes the dominant component. The occupation numbers for the first excited 2_1^+ states in the middle panel show a similar distribution as in the ground states. The bottom panel gives occupation numbers for the first excited 0_2^+ states. At

TABLE II: Calculated $B(E2)$ values for the positive-parity band built on the $9/2_1^+$ state in the odd-mass nuclei $^{53-59}$Cr.

	$B(E2)$ [e^2fm^4]			
$I_i^\pi \to I_f^\pi$	^{53}Cr	^{55}Cr	^{57}Cr	^{59}Cr
$13/2_1^+ \to 9/2_1^+$	143	283	260	360
$17/2_1^+ \to 13/2_1^+$	123	300	280	406
$21/2_1^+ \to 17/2_1^+$	58	172	126	361
$25/2_1^+ \to 21/2_1^+$	73	148	114	305

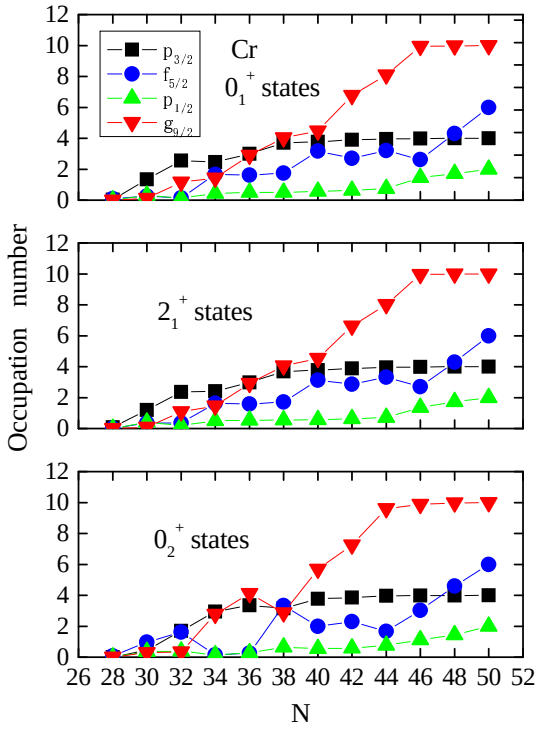

FIG. 14: (color online) Neutron occupation numbers of the fpg-shell orbits for three low-lying states in even-even Cr isotopes. (Upper panel) 0_1^+ states; (middle panel) 2_1^+ states; (lower panel) 0_2^+ states.

$N = 36$, we can see a peak of the $\nu g_{9/2}$ orbital in occupation number, and the $\nu p_{3/2}$ and $\nu g_{9/2}$ orbitals take almost the same occupation numbers. This means that the 0_2^+ state in ^{60}Cr consists of excitations from the $\nu p_{3/2}$ and $\nu g_{9/2}$ orbitals, and lies higher than that of $N = 34$. For $N = 38$, the three orbitals provide the collectivity. For the Cr isotopes beyond $N = 40$, the $\nu g_{9/2}$ orbital is the dominant component.

IV. CONCLUSIONS

We have carried out a comprehensive study for the structure of neutron-rich Cr isotopes using the spherical shell model. Overall, the calculated results are in good agreement with the experimentally known energy levels for even-even $^{52-62}$Cr and odd-mass $^{53-59}$Cr isotopes. Furthermore, a lowering of excitation energies for neutron-rich Cr isotopes at and beyond $N = 40$ has been predicted. We have explained several characteristic behaviors found in the calculation: (1) a rapid decrease of the $9/2_1^+$ energies for the odd-mass Cr isotopes with $N = 29 - 35$, (2) drastic structure changes at $N = 36$ with enhancement of the 0_2^+ energy and sudden reduction of the yrast band energy, and (3) steady decrease of the 2_1^+ energy in the smaller N region and the occurrence of pronounced collectivity around $N = 40$. Several interesting consequences associated with the subshell closure $N = 40$ have been discussed: (1) enhanced $B(E2)$ values, (2) lowering of the 0_2^+ energies, and (3) a new band with strong collectivity built on the 0_2^+ state in ^{64}Cr.

We have pointed out that the key ingredients to predict and explain these striking features are the monopole interactions. These attractive and repulsive interactions affect cooperatively the effective SPE. As we have seen in Fig. 2, the effective single-particle levels of $1p_{3/2}$, $0f_{5/2}$, and $0g_{9/2}$ approach to each other near $N = 40$, due to the monopole effects. It seems that the cooperative effects of this behavior and the many-body correlations enhance the collectivity near $N = 40$. On the other hand, the calculation without $1d_{5/2}$ (see Refs. [14] and [23]) does not lead to sufficient collectivity, which may suggest a need of including the $1d_{5/2}$ orbit in shell model calculations. It is an interesting open question why the problem has not settled down and how one can unify the different views. The attractive $\pi f_{7/2}$-$\nu f_{5/2}$ lowers the $f_{5/2}$ orbital with increasing N, and also provides the mechanism of lowering the 0_2^+ energy around $N = 40$. The attractive $\nu p_{3/2}$-$\nu g_{9/2}$ monopole interaction explains the rapid changes of structure at $N = 36$. Ge isotopes are considered as the mirror nuclei of Cr isotopes with respect to the $Z = 28$ shell closure. We have pointed out that the systematics of energy levels and $B(E2)$ values in Ge isotopes is quite similar to that in neutron-rich Cr isotopes. We thus expect that our model can explain the characteristic behaviors in Ge isotopes, and are applicable to the $N = Z$ nuclei with nuclear mass $A = 68 - 100$.

Y.S. is supported in part by the Chinese Major State Basic Research Development Program through grant 2007CB815005.

[1] R. V. F. Janssens, Nature (London) **435**, 897 (2005).
[2] R. Broda, *et al.*, Phys. Rev. Lett. **74**, 868 (1995).
[3] R. Grzywacz, *et al.*, Phys. Rev. Lett. **81**, 766 (1998).
[4] T. Ishii, *et al.*, Eur. Phys. J. A **13**, 15 (2002).
[5] O. Sorlin, *et al.*, Phys. Rev. Lett. **88**, 092501 (2002).
[6] K. Kaneko, M. Hasegawa, T. Mizusaki, and Y. Sun, Phys. Rev. C **74**, 024321 (2006).
[7] M. Hannawald, *et al.*, Phys. Rev. Lett. **82**, 1391 (1999).
[8] P. G. Reinhard, *et al.*, RIKEN Review, **26**, 23 (2000).
[9] H. Grawe and M. Lewitowicz, Nucl. Phys. **A693**, 116 (2001).
[10] K. Langanke, J. Terasaki, F. Nowacki, D. J. Dean, and W. Nazarewicz, Phys. Rev. C **67**, 044314 (2003).
[11] E. Padilla-Rodal, *et al.*, Phys. Rev. Lett. **94**, 122501 (2005).
[12] J. Van de Walle, *et al.*, Phys. Rev. Lett. **99**, 142501 (2007).
[13] M. Hasegawa, T. Mizusaki, K. Kaneko, and Y. Sun, Nucl. Phys. **A789**, 46 (2007).
[14] O. Sorlin, *et al.*, Eur. Phys. J. **A16**, 55 (2003).

[15] S. Zhu, *et al.*, Phys. Rev. C **74**, 064315 (2006).
[16] T. Otsuka, R. Fujimoto, Y. Utsuno, B. A. Brown, M. Honma, and T. Mizusaki, Phys. Rev. Lett. **87**, 082502 (2001).
[17] T. Otsuka, T. Suzuki, R. Fujimoto, H. Grawe, and Y. Akaishi, Phys. Rev. Lett. **95**, 232502 (2005).
[18] M. Honma, T. Otsuka, B. A. Brown, and T. Mizusaki, Eur. Phys. J. **A25**, s01, 499 (2005).
[19] S. Freeman, *et al.*, Phys. Rev. C **69**, 064301 (2004).
[20] A. N. Deacon, *et al.*, Phys. Lett. **B622**, 151 (2005).
[21] R. Grzywacz, *et al.*, Phys. Rev. Lett. **81**, 766 (1998).
[22] A. P. Zuker, J. Retamosa, A. Poves, and E. Caurier, Phys. Rev. C **52**, R1741 (1995).
[23] E. Caurier *et al.*, in ENAM2001, Eur. Phys. J. A **15**, 145 (2002).
[24] M. Hasegawa, K. Kaneko, and S. Tazaki, Nucl. Phys. **A688** (2001) 765.
[25] K. Kaneko, M. Hasegawa, and T. Mizusaki, Phys. Rev. C **66** 051306(R) (2002).
[26] E. Caurier, code ANTOINE, Strasbourg, 1989 (unpublished).
[27] J. I. Prisciandaro, *et al.*, Phys. Lett. **B510**, 17 (2001).
[28] R. V. F. Janssens, *et al.*, Phys. Lett. **B546**, 55 (2005).
[29] S. N. Liddick, *et al.*, Phys. Rev. C **70**, 064303 (2004).
[30] B. Fornal, *et al.*, Phys. Rev. C **70**, 064304 (2004).
[31] R. B. Firestone and V. S. Shirley, *Table of Isotopes*, 8th ed. (Wiley-Interscience, Nwe York, 1996).
[32] E. Caurier, F. Nowacki, and A. Poves, Nucl. Phys. **A742**, 14 (2004).
[33] M. Hasegawa, K. Kaneko, T. Mizusaki, and Y. Sun, Phys. Lett. **B656**, 51 (2007).
[34] M. V. Stoitsov, J. Dobaczewski, W. Nazarewicz, S. Pittel, and D. J. Dean, Phys. Rev. C **68**, 054312 (2003).
[35] M. V. Stoitsov, J. Dobaczewski, W. Nazarewicz, P. Ring, Comp. Phys. Comm. **167**, 43 (2005).